Bayesian Parameter Estimation for Arctic Coastal Erosion Under the Effects of Climate Change

Matthew Kupilik, *Member, IEEE*, Michael Ulmgren, and Dana Brunswick

***Abstract*—Arctic coastal erosion due to decreasing ice protection and increasing temperatures is a threat to coastal communities and infrastructure as well as a driver of long-term habitat changes. In order to respond to this threat, decadal predictive models are required that incorporate the effects of climate change under current emission trajectories. This work presents an Arctic erosion one-line model capable of estimating unknown coastal parameters through historic coastline measurements. Parameter estimation is carried out using both the extended and unscented Kalman filters, and the results compared. The model and parameter estimation are evaluated using two sections of Arctic coastline, one near Oliktok Point, AK, and the other along the coast of Barter Island, AK. Historic wave fields are modeled for both locations using downsampled historic GCM data for boundary conditions and estimating fetch distance. Future wave and temperature conditions are found using GCM projections under the RCP 8.5 pathway. Parameter estimation is performed on all coastal measurements except the most recent coastline available; this hold out measurement is then used to test the predictive power of the model. Coastlines at both locations are simulated from 1980 to 2070. It is found that root-mean-square error values for both locations are lower than purely empirical techniques and future predictions show increasing rates of erosion under the RCP 8.5 pathway.**

***Index Terms*—Arctic, Bayesian estimation, coastal erosion.**

I. Introduction

THE rapidly warming Arctic is leading to increased rates of Arctic coastal erosion, the large scale impacts of which are currently not well understood. As permafrost coastlines experience an increase in wave action due to a lengthening ice-free season combined with rapidly warming temperatures they are seeing erosion rates of up to 25 m per year [1]. Although such significant erosion is not observed at all permafrost coastlines, erosion is present over large portions [2]. The effects of such large scale erosion are being felt most immediately through the loss of coastal infrastructure along the sparsely populated coastline [3]. Coastal Arctic communities are also facing threats to subsistence hunting and fishing as well as damage to cultural sites [4]. Less researched are the impacts of Arctic erosion on marine habitats, both nearshore and on other connected marine ecosystems. Such impacts could include increased acidification and drastic changes in nutrient fluxes. On an even larger scale, Arctic coastal erosion could have impacts on global carbon fluxes, as permafrost coastline makes up a third of global coastline [5]. In order to investigate all of these impacts, predictive Arctic coastal modeling is required over large spatial (hundreds of kilometers) and temporal (tens of years) scales.

Arctic coastal erosion under the influence of climate change has been the focus of several modeling efforts. Modeling approaches can be classified according to the scales and processes they attempt to capture. Computationally expensive physics-based models are often used for modeling change on small spatial scales in response to events over short time frames. Generally, these include use of existing high-dimensional software packages capable of solving mass and energy balance equations that couple hydrodynamics, wave action, and sediment transport to determine coastal morphology. Such packages include Delft3D [6], [7] and XBeach [8]. It is possible to adapt these software packages to include Arctic specific erosional processes such as the effect of thawing permafrost and niche-erosion block collapse influenced by ice wedges, but such adaptations only increase the complexity. This complexity makes modeling over decadal time frames and hundreds of kilometers of varying coastline difficult.

Efforts in modeling Arctic specific processes directly include [9] and [10], which despite attempting a detailed process based model had difficulty recreating observed erosion rates over coastal segments of significant length. The models used in both [9] and [10] require very detailed knowledge about each coastline segment to be modeled, including bluff profiles, soil composition, and location of ice wedges. As such, neither of these works were applied to long sections of coastline. More empirical approaches include [11] and [12]. The latter uses historical coastlines and hindcasted GCM data to train a Gaussian process (GP) model that utilizes forecasted GCM data to estimate erosion rates. This machine learning method scales well and does not require detailed knowledge about soil composition, coast profile, or ice wedges. It does require a large volume (tens of years) of observed coastline change that can be used to infer the relationships between increasing temperatures and erosion rates. It is used as a comparison for the work presented here. Regardless of approach, all are limited by the dearth of training and validation data available compared to other coastal regions impacted by climate change.

Manuscript received May 4, 2020; revised June 10, 2020; accepted June 18, 2020. Date of publication June 22, 2020; date of current version July 5, 2020. This work was supported by the U.S. Air Force under the U.S. Army Corps of Engineers under Contract W911KB-14-2-0001. *(Corresponding author: Matthew Kupilik.)*

Matthew Kupilik is with the Department of Electrical Engineering, University of Alaska Anchorage, Anchorage, AK 99508 USA (e-mail: mkupilik@alaska.edu).

Michael Ulmgren and Dana Brunswick are with the Civil Engineering Department, University of Alaska Anchorage, Anchorage, AK 99508 USA (e-mail: nulmgren@alaska.edu; dinjerd@alaska.edu).

Digital Object Identifier 10.1109/JSTARS.2020.3004291

For this work, we adapt the one-line modeling approach used in [13] to include a thermoerosional component. Vitousek *et al.* [13] applied a one-line model using GCM-based driver data to California coastlines. The spatial and temporal timescales are very similar to the desired scales we are trying to apply in Alaska. Erosion rates are calculated along a series of transects based off beach slope, composition, and wave action. Parameters for individual transects were allowed to vary and estimated using an extended Kalman filter (EKF), using the method developed in [14]. We adapt much of this model structure, adjusting some terms to allow for the Arctic specific processes as the model was designed for use in California, which is not subject to permafrost thawing and the block niche erosion. We also determine the effectiveness of the linear assumption implicit in the choice of the EKF by comparing results to those obtained using an unscented Kalman filter (UKF).

Fig. 1. Transects for Oliktok study section and Alaska location (inset).

Fig. 2. Transects for Barter Island study section and Alaska location (inset).

II. Methodology

Arctic coastal erosion is a complicated high-dimensional physical process. Erosion rates are a nonlinear function of wave action, temperature (air, water, and soil), the permafrost structure, bluff profile, and others. In order to model over the desired spatial and temporal scales, a significant reduction in complexity is required. A common approach is to discretize the coastline into a series of transects, each perpendicular to some discrete spatial piece of coast. Modeled coastlines are then restricted to intersection points at each transect. Such an approach reduces the number of spatial dimension to one, but precludes the ability to model phenomena such as spit and island formation. We break the two study areas in this work into transects spaced approximately 50 m apart, and restrict the coastline to intersections with these transects (see Figs. 1 and 2). The Barter Island study section consists of 103 transects, and the Oliktok study section consists of 173 transects.

In order to calculate coastal positions along transects, the change in coastal position with respect to time at each transect is defined as (1) shown at the bottom of this page. This governing equation is applied to each transect individually. Y is the position along the transect in meters and t is the time, discretized using a timestep of one day. The first three terms, longshore, cross-shore, and sea level, on the right-hand side are unchanged from [13], we make use of their notation and as such they are described only briefly. The final term is designed to capture effects from decreasing sea ice and increasing temperatures and is a modification from the model in [13].

The first term represents longshore sediment transport where Q is the longshore sediment transport rate, d is the depth of closure, and X is the horizontal distance (discretized to the transect spacing). The sediment transport rate Q is found as a function of the input wave field (height and angle) and its relation to the current shoreline position.

C is a coefficient for cross-shore transport and E is the wave energy, which is directly mapped to wave height. The formulation is according to [15]. ΔE is the energy mismatch between the instantaneous wave energy and the energy associated with the equilibrium position. The equilibrium energy is empirically found using as a linear function from the current shoreline position Y_{st}

$$E_{\text{eq}} = aY_{st} + b \tag{2}$$

$$\frac{\partial Y}{\partial t} = \underbrace{-\frac{1}{d}\frac{\partial Q}{\partial X}}_{\text{Longshore}} + \underbrace{C\sqrt{E}\Delta E}_{\text{Cross-shore}} - \underbrace{\frac{c}{\tan\beta}\frac{\partial S}{\partial t}}_{\text{Sea level}} + \underbrace{V_t\frac{H^{\cdot 8}}{\tau}(T_w - 1.8)}_{\text{Thermoerosional}} \tag{1}$$

where a and b are empirical parameters estimated using the Kalman filter.

The third term allows for changes in coastal position due to sea level rise (SLR). Variables in this term include c, an empirical parameter, $\tan\beta$, the beach slope, and S, the level of sea rise. The slope is also filtered using a second-order Butterworth low-pass filter with a cutoff frequency of 0.01. This aggressive filter is used as the calculated beach slope shows unreasonable variation along transects as it is found from course 2-m digital elevation model (DEM) data [16]. Per [13], we hold the beach slope for each transect constant, as the foreshore slope only, in order to minimize the Bruunian response [17], [18]. Block collapse events are not directly modeled and collapsed blocks erode quickly relative to the prediction time frame [10]; thus, we do not include these when calculating beach slope.

In order to include Arctic specific effects, including increased erosion rates due to decreasing ice protection and thawing permafrost we include a fourth term. V_t is an empirical parameter, H is the wave height at a transect (daily mean), τ is the wave period (daily mean), and T_w is the nearshore water temperature. 1.8 is an offset for the freezing temperature of sea water. This parameterization follows [19] and was chosen based off the analysis in [10], which compared the White formulation to other mechanisms of block erosion, including [20] and [21]. The White formulation was found to most closely match observed bluff retreat rates near Drew Point, AK. The original White formulation contains the product of two unit-less empirical constants and a surface roughness coefficient that has units of meters$^{0.2}$. Since this roughness coefficient is unknown and can vary spatially, we include it within the V_t empirical parameter. The V_t term encapsulates many of the physical properties of the bluff that are unknown at most transects. It also acts as a weighting to the combined impact of increasing wave action and rising temperatures.

The resulting nonlinear differential equation is solved using a forward Euler method, discretized with a time step of one day. Temporally discretizing into n timesteps and splitting the equations into $Y = Y_{st} + Y_{lt}$ as per [13] and [14] results in the following equations:

$$\frac{Y_{st}^{n+1} - Y_{st}^{n}}{\Delta t} = C(E^n)^{\cdot 5}(E^n - aY_{st}^n - b) \tag{3}$$

$$\frac{Y_{lt}^{n+1} - Y_{lt}^{n}}{\Delta t} = -\frac{K}{d}\frac{Q^{n+1} - Q^n}{\Delta X} - \frac{c}{\tan\beta}\left(\frac{\partial S}{\partial t}\right)^n + \epsilon \tag{4}$$

$$\epsilon = V_t \frac{(H^n)^{\cdot 8}}{\tau}(T_w^n - 1.8). \tag{5}$$

Equations (3)–(5) are solved individually at each transect. ΔX is the spatial discretization, or the distance between transects. The thermoerosional component is given as ϵ. The longshore erosion component Q is calculated at a half transect spacing as well in order to maintain continuity at neighboring transects.

Arctic erosion is often storm driven and highly episodic, the model is formulated to capture approximations to these difficult to model events that are often weather driven. Inputs to the model are found using forecasted GCM data, which although statistically representative of impacts to weather due to climate change does not attempt to provide an accurate day by day breakdown. This approach is valid as we are only attempting to observe results over multiple decades as compared to predicting coastline response to single storm events that can occur on time frames less than our time step. An additional strength of this method is that it can be applied to coastal transects of very different types through either manual adjustment of constants or more rigorously (as most constants are not known over long coastlines) by utilizing a recursive Bayesian filter, such as an extended Kalman to update estimates of each parameter as new measurements become available.

TABLE I
WINDSPEED THRESHOLDS (METERS PER SECOND) FOR SYNTHETIC STORMS

	West Storm	East Storm
Medium	8.5 to 9.6	8.5 to 9.94
High	9.6 or greater	9.94 or greater

A. Model Inputs

The nonlinear relationship in (1) requires knowledge of the wave field and shoreline, both composition and slope. Much of this information is difficult to obtain over Alaska coastlines and can vary significantly over the modeled transects. Parameters that are generally unknown and can vary both temporally and spatially are split into a state vector and estimated using a Kalman filter. Known variables that act as forcing parameters are classified as inputs. This section describes the method used for calculating the wave climate, determining beach slope, SLR, and nearshore water temperature, which act as drivers to the model.

For modeling wave climate we made use of Delft3D [6]. As our modeling time period spans 1979 to 2070, modeling the entire time period, even with a daily timestep is not feasible. As such we modeled a series of representative storm events over the time period, and used forecasted GCM wind vector data to determine when those premodeled storm events occur. We make use of a composite of downscaled wind vectors from GCM models: NCAR-CCSM4 [22], GFDL-CM3 [23], GISS-E2-R [24], IPSL-CM5A-LR [25], and MRI-CGCM3 [26]. Modeled storm events are classified using direction and intensity, resulting in four types of resulting in four types of storms, shown in Table 1. Each of these four storms was modeled under various ice conditions expected to be present during specific months. An average open water extent for each open water month was determined decadally. The historical data source for determining open water extent is 25-km resolution, monthly-averaged sea ice extent data from the National Snow and Ice Data Center. Based on the historic record, the open water period has mainly been limited to July–October. Therefore, synthetic storms were only modeled for those months during the historic periods. GCM forecast data indicates that open water can be expected into the month of November in the future. Therefore, future decadal periods (2021–2070) also include the month of November. Within Delf3D-Flow, ice was represented in the form of floating structures, whereas the nested wave grids within Delft3D-Wave were adjusted based off the estimated open water extent.

The resulting nearshore wave height and period are required when determining the longshore sediment transport rate Q as

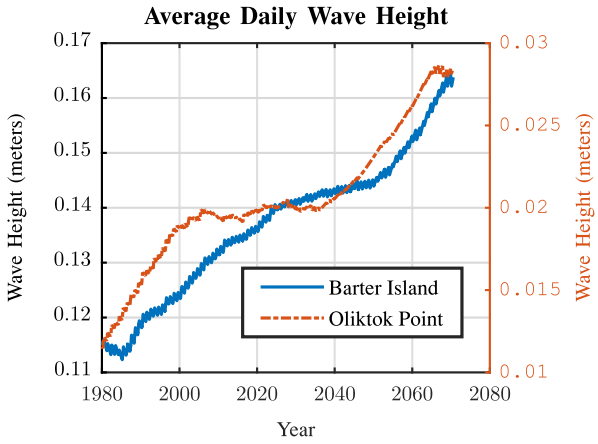

Fig. 3. Average daily wave heights versus time for both study locations.

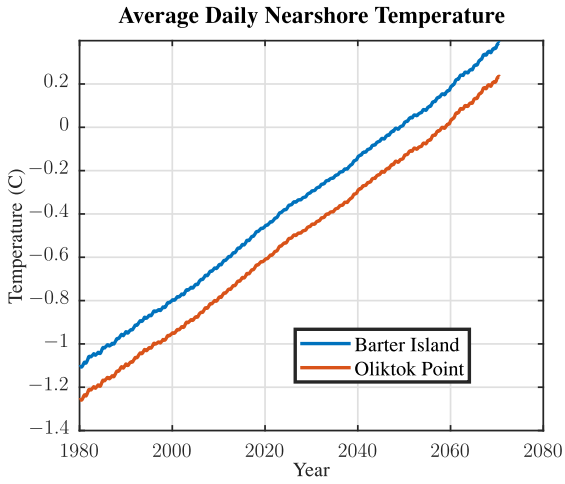

Fig. 4. Average daily nearshore temperature versus time for both study locations.

well as used directly in the thermoerosional term. Short-term changes in sea level due to storm surge are not directly modeled. Under the GCM 8.5 pathway, both locations are expected to see increased wave action over time. Fig. 3 shows the average daily wave heights throughout the study time frame. This average is calculated over ice and ice-free periods so actual wave height observed during storm events is much higher (particularly at Oliktok). The amount of wave energy impacting both coastlines is expected to increase over the prediction period.

Beach slope is determined from public 2-m DEM data [16]. The coastal profile is generated by interpolating at 1000 equidistant points along each transect. We then fit a line to a restricted region from 5 m below sea level to 3 m above, the beach slope is then found as the angle of this line. The resulting beach slope is not used for any bluff or block erosion inputs, but is used for longshore sediment transport. The resulting angle can vary quite widely at neighboring transects so it smoothed, resulting in an average beach slope of $1:80$ at Oliktok and $1:7$ at Barter Island. As most of the Oliktok coastline is bluffline, only the strip below the bluff is considered, resulting in a low average slope. Barter Island by contrast has a significant beach section along the east end of the study area.

SLR, although not predominant, is still included in the model. Northern Alaska is experiencing a small amount of SLR in contrast to southern Alaska where glacier heavy regions are rebounding. In order to project SLR, we use the projections in [27]. We assume an annual SLR of 1.0 mm per year. Larger values, up to 5.0 mm per year were tested and still found to have a negligible impact on erosion rates.

Nearshore water temperature is also required for the thermoerosional component of the model. We again utilize downsampled GCM data from the same sources described previously. Increasing nearshore water temperatures are also expected for the GCM 8.5 pathway, as shown in Fig. 4.

III. Parameter Estimation

Equation (1) results in a nonlinear differential equation with respect to time. In order to solve this differential equation, knowledge of all unknown parameters not classified as inputs are grouped into a state-space formulation. The state vector is defined as $\psi = [Y_{lt} \;\; V_t \;\; Y_{st} \;\; C \;\; a \;\; b \;\; c \;\; K]^T$, where we again borrow the notation from [13]. This formulation results in a set of eight nonlinear equations, given in (8) shown at the bottom of the next page. The scalar output is the new distance along each transect, given in (9) shown at the bottom of the next page. These equations must be solved individually for every single transect, thus each transect has a unique state vector containing the parameters to be estimated; however, only Y_{lt} and Y_{st} are expected to vary temporally. The remaining states are included in the state vector as they are unknown and need to be estimated. To perform this estimation we make use of both the extended Kalman and the UKFs. Any Bayesian filter could be applied, but computational efficiency is a concern as the Barter Island study area has 103 transects and the Oliktok study area has 173 transects, so we are required to update 276 filters every time a new measurement is obtained.

A. Extended Kalman Filter

In order to apply an EKF the state equation must be linearized, as the distributions of all parameters are assumed to be Gaussian. The Jacobian can be found symbolically. The only terms in the 8×8 matrix modified from [13] are given in (6) and (7). Where F_1 is the discretized solution to (4) and (5). The state equations are also augmented using exponents to maintain negative signs on C, a and positive signs on b, c, and K; for details, see [13, Appendix B].

$$F_1 = Y_{lt} - \Delta t \left(\frac{K}{d} \frac{Q^{n+1} - Q^n}{\Delta X} - \frac{c}{\tan \beta} \left(\frac{\partial S}{\partial t} \right)^n + \epsilon \right) \tag{6}$$

$$\frac{\partial F_1}{\partial V_t} = -\Delta t \frac{(H^n)^{.8}}{\tau} (T_w^n - 1.8) \tag{7}$$

The initial covariance matrix P is set to estimate uncertainty in specific parameters. The process noise Q and measurement noise R are generally set to weight measurements, as we want to force the parameters to match our observations. Initial values of P and

Q are given in (10) and (11) shown at the bottom of this page. The measurement noise, $R = 1$. The covariance associated with the Bruunian response c is set to essentially make it constant. This decision follows [13] as SLR is expected to be small at both study locations.

Initial means vary for each transect at each study area. The initial long-term position, Y_{lt} is set to the earliest coastal position available. The short term component, Y_{st} is set to zero for all transects. The thermoerosional constant V_t is set by taking the earliest position together with the associated wave and water inputs (H, τ, and T_w) then calculated directly from (4) and (5), assuming contributions from all other model components are zero. The cross-shore coefficient C is initially set to -0.5 for all transects. The two empirical parameters relating the short term position to the equilibrium energy, a and b, are set to $a = -0.1$ and b as the average of the wave height over the study time frame. The Bruunian coefficient c is set to 1.0 and not allowed to change. The coastline transport coefficient K is set to 100 for all transects.

B. Unscented Kalman Filter

The UKF [28] was designed to overcome some of the limitations of the EKF, particularly the reliance on a first-order linear approximation of the dynamics. The UKF uses a statistical linearization, passing a set of states (known as sigma points) through the nonlinear dynamics and fitting a distribution to the result. The UKF is capable of capturing the posterior mean and covariance for any nonlinearity up to a second-order Taylor approximation. This increase in accuracy also does not increase the overall complexity of the filter. We make use of the UKF in order to validate the linear approximation made using the EKF. For the UKF implementation all variables are still modeled as Gaussian random variables and we make use of the same initial mean and covariance as in the EKF case.

C. Measurements

The measurements used to adjust the state parameters consist of coastlines intersected with all transects. The Arctic has very few coastal surveys and we are forced to train our model using all the available measurements except the most recent, which is held out for validation. Coastlines are extracted from a variety of sources, historic coastlines are from the USGS National Assessment of Shorelines project [29] or provided directly by the U.S. Air Force (USAF). More recent coastlines have been manually extracted from orthorectified satellite imagery provided by [30] or GPS coastline measurements. For coastlines extracted from imagery, we made use of the sea–land interface. Although this is subject to short term change it is acceptable in this case as the tidal ranges are quite low at both study areas [29]. Measurements and sources are summarized in Table II.

TABLE II
COASTAL POSITION DATA

Barter Island		Oliktok	
Year	Source	Year	Source
7/13/1979	USGS Orthoimagery	7/15/1979	USGS Orthoimagery
8/29/2003	USGS Quickbird	7/1/2004	USGS Orthoimagery
9/05/2009	USGS LIDAR	7/30/2005	USAF
7/17/2010	USGS LIDAR	6/09/2009	USAF
6/28/2011	Planet [30]	7/30/2009	USAF
7/27/2012	Planet [30]	7/25/2010	USGS LIDAR
7/19/2013	Planet [30]	8/04/2010	USGS LIDAR
8/16/2016	GPS/GEO XT 6000	6/27/2011	Planet [30]
8/27/2016	Planet [30]	7/22/2012	Planet [30]
7/17/2017	NOAA Orthoimagery	7/21/2013	Planet [30]
9/20/2018	Digital Globe	7/30/2014	Planet [30]
		7/04/2015	USGS
		8/06/2016	Planet [30]
		7/13/2017	Planet [30]
		8/19/2018	Digital Globe

IV. RESULTS

The primary objective of the model is to be able to accurately predict coastline positions in the Arctic decades into the future under the effects of climate change. This section will discuss the ability of the model to make predictions at the two study areas into the future. The secondary model objective is to evaluate the effectiveness of the EKF and the linearization compared to the UKF.

$$\frac{\psi^{n+1}-\psi^n}{\Delta t} = \begin{bmatrix} -\frac{K}{d}\frac{Q^{n+1}-Q^n}{\Delta X} - \frac{c}{\tan\beta}\left(\frac{\partial S}{\partial t}\right)^n + V_t\frac{(H^n)^{\cdot 8}}{\tau}(T_w^n - 1.8) \\ 0 \\ C(E^n)^{\cdot 5}(E^n - aY_{st}^n - b) \\ 0 \\ 0 \\ 0 \\ 0 \\ 0 \end{bmatrix} \tag{8}$$

$$Y^n = [1 \quad 0 \quad 1 \quad 0 \quad 0 \quad 0 \quad 0 \quad 0]\,\psi^n \tag{9}$$

$$P = \text{diag}\left(\begin{bmatrix} 1 & 0.2 & 1 & 0.01 & 0.01 & 0.01 & 1\times10^{-20} & 0.1 \end{bmatrix}\right) \tag{10}$$

$$Q = \text{diag}\left(\begin{bmatrix} 0.01 & 1\times10^{-10} & 0.01 & 1\times10^{-6} & 1\times10^{-6} & 1\times10^{-6} & 1\times10^{-20} & 1\times10^{-8} \end{bmatrix}\right). \tag{11}$$

TABLE III
RMSE COMPARISON (METERS)

	Study Site	
Method (Abbreviation)	Barter Island	Oliktok
UKF	22.43	6.34
EKF	24.19	5.93
GP	26.61	6.30
LR	35.76	5.58

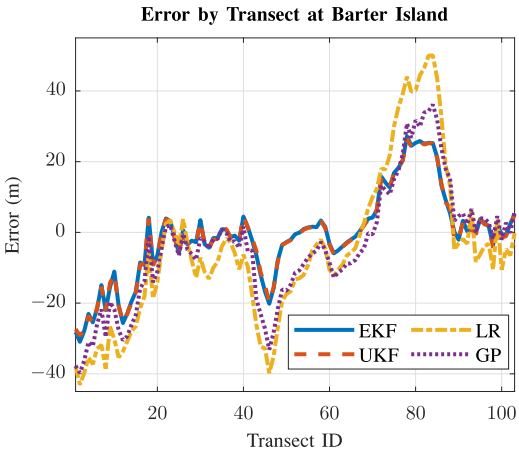

Fig. 5. Difference between model predictions and measured coastline position by transect at Barter Island. Compared models are the EKF, UKF, LR, and GP.

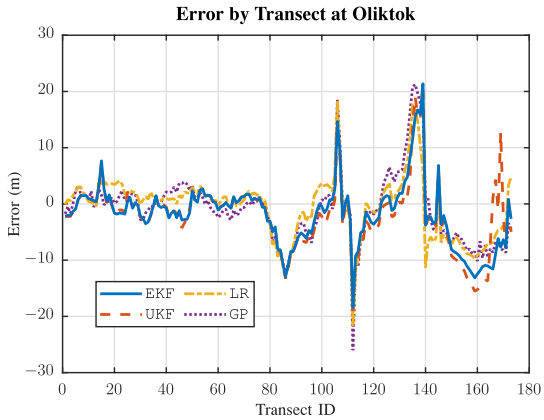

Fig. 6. Difference between model predictions and measured coastline position by transect at Oliktok. Compared models are the EKF, UKF, LR, and GP.

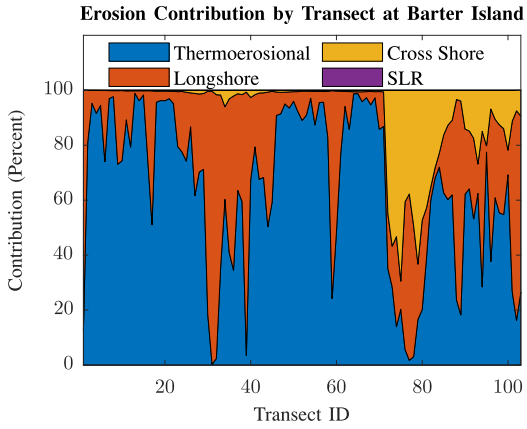

Fig. 7. Model component contribution (percent of total erosion) by transect at Barter Island (1980–2070). The contribution from SLR is negligible.

A. *Coastal Predictions*

The model is run at each study location using a daily timestep, whenever a measurement is available the information is used to update the values of the unknown constants contained within the state vector. All measurements except the most recent are used for training. The model then begins prediction when no further measurements are available. In order to determine the root-mean-square error (RMSE), model predicted shoreline positions are compared to the measured shoreline positions at the most recent year, 2018 for Barter Island and 2018 for Oliktok. RMSE is found as

$$\text{RMSE} = \sqrt{\frac{\sum_{i=1}^{n}(P_i - M_i)^2}{n}} \tag{12}$$

where n is the total number of transects, P_i is the model predicted position for transect i, and M_i is the measured coastline position for transect i. Error results are summarized in Table III. Model results are compared to linear regression (LR), which does not take into account any inputs outside time and the GP method detailed in [12]. The GP is a data-driven approach that does take into account limited GCM climate inputs (increasing temperature). The predictive ability of the model varies depending on the study location but consistently outperforms the purely empirical techniques. The errors in meters for all models across both study areas by transect are shown in Figs. 5 and 6, where positive error implies the model over estimated erosion, and negative error implies the model under estimated erosion. These errors are the same as those used to find the total RMSE error for all models (12), only displayed spatially. The errors at Barter Island are dominated by the predominantly beach sections at the far east and western transects (approximately transects 1–20 and 75–103). This error is most likely due to an overreliance on the thermoerosional model component, which, although reduced at those transects, is still a significant source of erosion, as shown in Fig. 7. We expect that increased training data would improve this mismatch. The eastern beach transects are also undergoing deposition as a barrier island migrates westward and provides protection from increased wave action. Although we included expected changes to bathymetry, this migration is expected to continue into the future and contributes to the error on the eastern quarter of the study section. Historically (1979–2019), the Barter Island study area has experienced a mean loss of 1.73 m per year on those transects experiencing net erosion. Over the forecast period (2020–2070), the rate is expected to increase to a mean loss of 2.38 m per year.

At Oliktok, erosion rates are approximately linear up to 2017; this is shown by the low RMSE for the LR (see Table III). The model captures this linearity, although the differences between the two are within the expected noise of the measurement itself. The same noise floor holds for comparisons between the EKF/UKF and the GP model, all are within a meter. The Oliktok study section also consists of mostly uniform permafrost bluff, which is confirmed by the much greater reliance on the

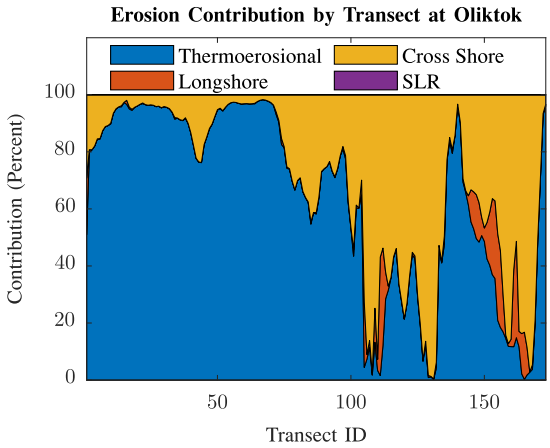

Fig. 8. Model component contribution (percent of total erosion) by transect at Oliktok (1980–2070). The contribution from SLR is negligible.

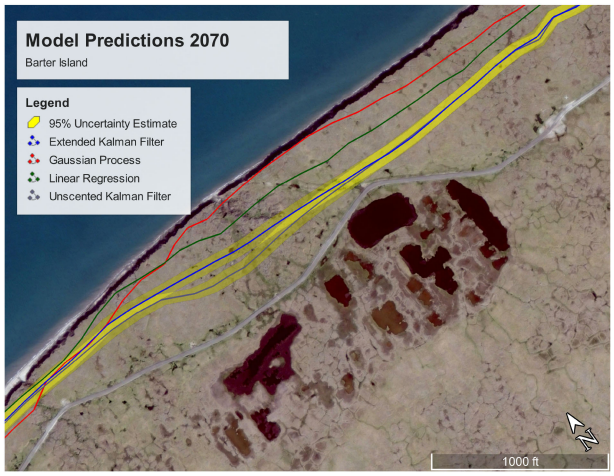

Fig. 9. Long-term model comparison for 2070 at a representative section (transects 46–74) of Oliktok. Included models are the EKF, UKF, LR, and GP. The 95% uncertainty bounds are not shown as they are within the line width (approximately 3 m).

thermoerosional component, as shown in Fig. 8. Historically, the Oliktok study area has experienced a mean loss of 0.83 m per year on those transects experiencing net erosion. Over the forecast period (2020–2070) the rate is expected to increase to a mean loss of 1.24 m per year. This reduction in erosion rate compared to Barter Island matches the reduction in predicted wave action compared to Barter Island under the GCM 8.5 pathway.

V. Discussion

There is essentially no difference in measured predictive ability between the Bayesian filters, which implies that the locally linear assumption made by the extended Kalman is valid over annual time frames. The similarities are prominent at the Oliktok study site, with the predicted coastlines almost indistinguishable out to 2070, as shown in Fig. 9. At Barter Island however, the UKF generally predicts an increase in the amount of erosion when compared to the EKF, as shown in Fig. 10.

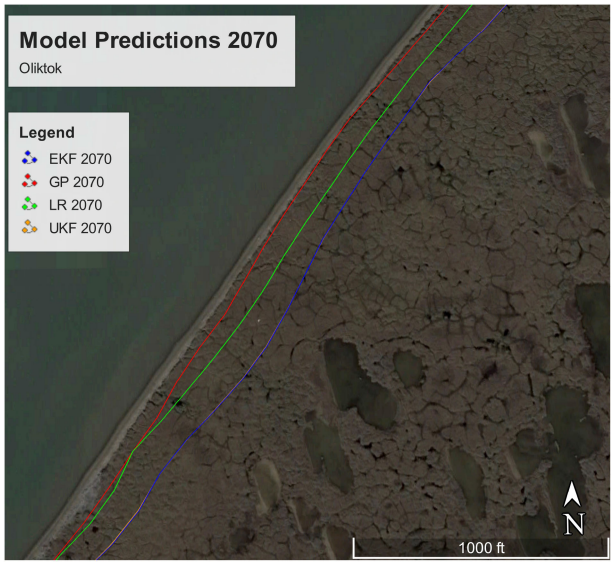

Fig. 10. Long-term model comparison for 2070 at a representative section (transects 37–67) of Barter Island. Included models are the EKF, UKF, LR, and GP. The 95% uncertainty bounds are shaded yellow for both the EKF and UKF.

There was additionally no change in model component contribution (see Figs. 7 and 8). Both filters were stable, the covariance matrix for both converges within a few updates.

The converged values for each state by transect are shown in Fig. 11 for the five parameter (empirically fit) states. Note that c is excluded as the SLR has a negligible impact on erosion rates and c is not allowed to change. These results are presented only for the Oliktok study section as it had the largest number of measurements at each transect, thus giving the filter more time to converge and a better standard of comparison between the EKF and UKF. Both Kalman filters introduce significant variability in parameters across transects. The rapid changes in the K parameter near transect 100 are due to actual changes in grain size and sediment type as well as the model compensating for unmodeled dynamics (such as a small revetment). Most other parameters vary smoothly with the exception of the far east end (transects 175 and up). These large changes are due to the model attempting to compensate for artificial structures. The resulting 95% position uncertainty for both the UKF and EKF is approximately 25 m at Barter Island (see Fig. 10) and 3 m at Oliktok.

There is a measurable difference in the variance related to the K term. This term acts as a weight on the longshore erosion component, which is highly nonlinear due to trigonometric functions within the calculation of Q. The magnitude of difference is relatively small, but over long simulation time periods can result in differences between the UKF and EKF when longshore erosion is weighted highly. This difference (see Fig. 10) is shown by the increased difference between the EKF and UKF at Barter Island, where the impact of longshore erosion is greater than that at Oliktok, shown by Figs. 7 and 8. The K parameter also has the largest differences in final value between the two filters.

Final variances (after the last measurement is received) are shown for select states as a function of transect in Fig. 12.

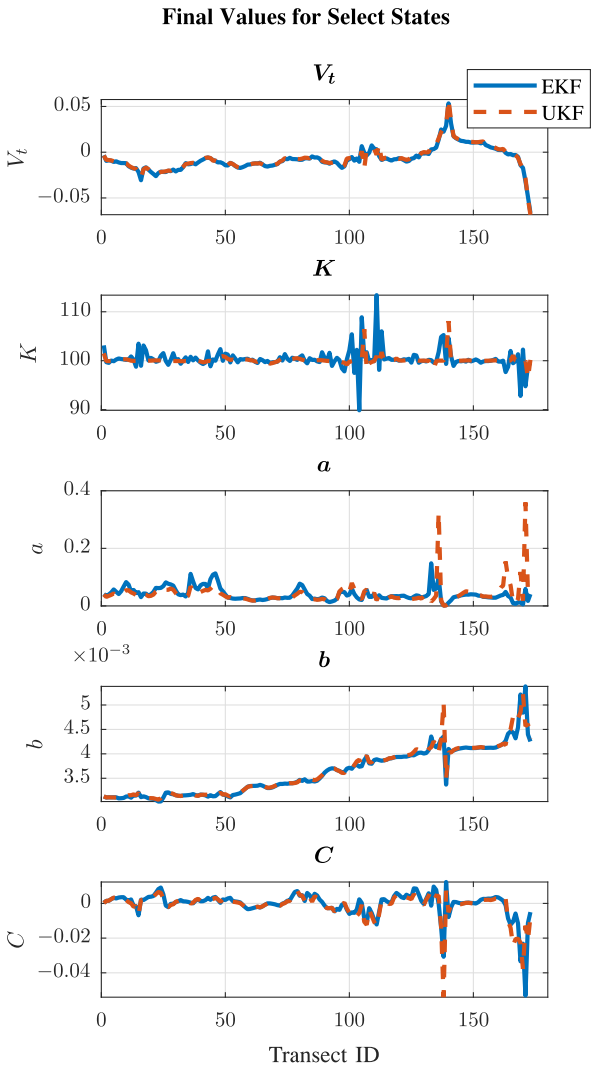

Fig. 11. Final values of select states by transect for the EKF and UKF at Oliktok.

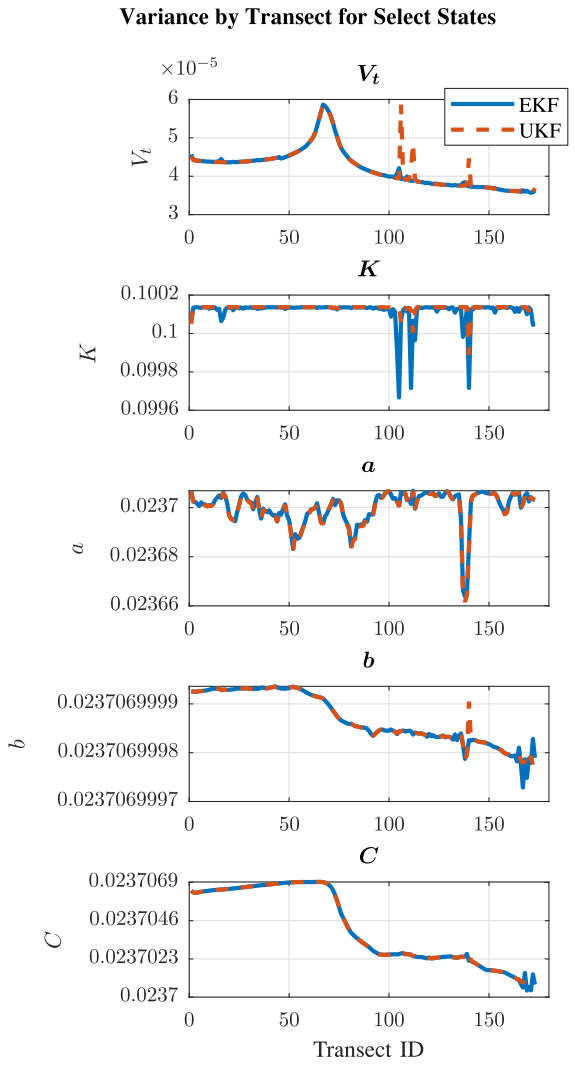

Fig. 12. Final variance of select states by transect for the EKF and the UKF at Oliktok.

Differences are shown spatially and indicate where the filters have differences in capturing variances at individual transects. The UKF shows spatially localized spikes in the variance of the thermoerosional term V_t. These spikes occur at transects 106–107, 111–112, and 140. These locations all correspond to regions where the model is expected to miss localized dynamics. Transects 106–107 are located along a stream outlet that requires a spatial interpolation to predict a coastline across. Over the training time frame, this outlet has moved, which is not modeled. Transects 111–112 are located immediately after a manufactured revetment, which was built during the later part of the training period. The revetment transects themselves are constant, but the introduction of the revetment changed how the neighboring transects react. Finally, transects 140–146 are the location of an industrial facility and have a fixed coastline. Over the validation time frame, the UKF does no better at capturing the impacts of these unmodeled dynamics, but it does capture the increased variance in the states due to the increased mismatch between observation and model prediction given expected inputs. It is possible to simply exclude these transects from analysis but we opted to leave them in in order to see if either Kalman filter can empirically adjust the constants to match unmodeled dynamics. The flexibility to apply the method to a wide range of transects is a benefit of the approach.

The similarity in variance for the C, a, and b parameters is due to all three being part of the cross-shore erosion term. All three parameters show a high covariance at transects where the model predicts significant cross-shore erosion. This similarity does not imply identical values for the constants but rather that the model has trouble differentiating which constants to update given a change in expected cross-shore erosion; these states are weakly observable. Since all three start with similar initial variances, all three converge to similar values. It is possible the model could collapse these states and not lose a significant amount of predictive power.

Observability is a problem for the convergence of both filters. As discussed in [14], choice of initial states and priors is important. As the system studied is linearized around the current estimate at every update, an approximation of observability can be calculated over a time period using the partial observability

matrix presented in [31]. When this observability matrix is calculated using all measurements from the Oliktok study site, the resulting rank is only 2. This rank deficiency indicates that a state vector cannot be uniquely calculated for a given set of measurements and inputs for the linearized model over the update period. Solutions to this are challenging for the presented model using only coastal positions as a measurement. The ability to differentiate long-term coastal changes due to bluff erosion (thermoerosional) versus cross and longshore sediment transport would be required to increase the observability. As these rates vary tremendously across transects this measurement would require more detailed imagery (or increased field work) over whatever study areas are chosen.

The difficulty in uniquely calculating model states from measurements is not only a problem for the Bayesian filters applied to the one-line model presented here. As increasingly complex models are designed to include a larger variety of physical mechanisms, such as niche erosion and block collapse, additional model parameters are required, such as grain size, ice content, and bluff profile. If those parameters cannot be learned from observations they need to be estimated from field measurements. These parameters can vary widely across Arctic coastlines of interest, quickly making sampling and validating measurements infeasible due to logistics and weather. It is thus a tremendous benefit to tailor model complexity such that dominant dynamics can be represented and parameters can be estimated from obtainable measurements.

VI. Conclusion

We have demonstrated that the inclusion of wave and thermoerosional effects into simplified long-term one-line Arctic coastal models can significantly improve prediction accuracy when compared to purely empirical techniques. The model decreased prediction error along the Arctic coastal bluff and beach lines by 31%. The drawback to this modeling approach over the presented empirical methods is that the localized wave climate must be modeled over the entirety of the prediction period. For large coastlines, this requires a significant effort. As we are using statistically expected climate conditions to drive localized wave models, such models are also valid only over annual to decadal time frames.

The comparison of the EKF and UKF filters has shown that the linearization implicit in the EKF is valid over our short validation period. Very little difference was seen in the state estimates from the two filters. Over long prediction time frames, however, the UKF showed higher rates of erosion, particularly at transects with a higher longshore erosion component. The changes in variance (and as a result uncertainty in the output) between the two filters is small, but not undetectable.

For our implementation, the EKF is computationally faster than the UKF as the Jacobian was found symbolically. The UKF required a full nonlinear model evaluation for each sigma point, which slowed it considerably. The EKF suffers from the same complexity if the Jacobian must be found numerically.

The loss of Arctic coastlines is having an immediate impact on many communities, a currently unknown impact on marine and nearshore environments, and a potential impact on carbon fluxes planet wide. Future work will include refining such models to include variable coastal profiles while at the same time expanding the lengths of coastlines to be modeled.

Acknowledgment

The authors would like to thank Dr. S. Vitousek for providing them with the code for COSMOS-COAST. They acknowledge the World Climate Research Programme's Working Group on Coupled Modelling, which is responsible for CMIP, and they thank the climate modeling groups for producing and making available their model output. For CMIP, the U.S. Department of Energy's Program for Climate Model Diagnosis and Intercomparison provides coordinating support and led development of software infrastructure in partnership with the Global Organization for Earth System Science Portals. The views and conclusions contained in this document are those of the authors and should not be interpreted as necessarily representing official policies, either express or implied, of the U.S. Air Force or U.S. Army Corps of Engineers.

References

[1] B. M. Jones *et al.*, "A decade of remotely sensed observations highlight complex processes linked to coastal permafrost bluff erosion in the Arctic," *Environ. Res. Lett.*, vol. 13, no. 11, 2018, Art. no. 115001.

[2] A. E. Gibbs and B. M. Richmond, "National assessment of shoreline change—Historical shoreline change along the North Coast of Alaska, U.S.–Canadian border to Icy Cape," Open File Report, U.S. Geological Survey, Reston, VA, USA, 2015.

[3] J. M. Frederick, M. A. Thomas, D. L. Bull, C. A. Jones, and J. D. Roberts, "The Arctic coastal erosion problem," Sandia Nat. Lab., Albuquerque, NM, USA, Tech. Rep. SAND2016-9762, 2016.

[4] B. M. Jones, K. M. Hinkel, C. D. Arp, and W. R. Eisner, "Modern erosion rates and loss of coastal features and sites, Beaufort Sea coastline, Alaska," *Arctic*, vol. 61, no. 4, pp. 361–372, 2008.

[5] H. Lantuit *et al.*, "The Arctic coastal dynamics database: A new classification scheme and statistics on Arctic permafrost coastlines," *Estuaries Coasts*, vol. 35, no. 2, pp. 383–400, 2012.

[6] G. R. Lesser, J. A. V. Roelvink, J. A. T. M. Van Kester, and G. S. Stelling, "Development and validation of a three-dimensional morphological model," *Coastal Eng.*, vol. 51, no. 8/9, pp. 883–915, 2004.

[7] P. D. B. Crespo *et al.*, "Sediment budget analysis of the Guayas River using a process-based model," *Hydrol. Earth Syst. Sci.*, vol. 23, no. 6, pp. 2763–2778, 2019.

[8] D. Roelvink, A. Reniers, A. P. van Dongeren, J. van Thiel de Vries, R. McCall, and J. Lescinski, "Modelling storm impacts on beaches, dunes and barrier islands," *Coastal Eng.*, vol. 56, no. 11/12, pp. 1133–1152, 2009.

[9] M. A. Hoque and W. H. Pollard, "Arctic coastal retreat through block failure," *Can. Geotech. J.*, vol. 46, no. 10, pp. 1103–1115, 2009.

[10] K. R. Barnhart, R. S. Anderson, I. Overeem, C. Wobus, G. D. Clow, and F. E. Urban, "Modeling erosion of ice-rich permafrost bluffs along the Alaskan Beaufort Sea coast," J. Geophys. Res., Earth Surface, vol. 119, no. 5, pp. 1155–1179, 2014.

[11] T. M. Ravens, B. M. Jones, J. Zhang, C. D. Arp, and J. A. Schmutz, "Process-based coastal erosion modeling for Drew Point, North Slope, Alaska," *J. Waterway, Port, Coastal Ocean Eng.*, vol. 138, no. 2, pp. 122–130, 2012.

[12] M. Kupilik, F. D. W. Witmer, E.-A. Macleod, C. Wang, and T. Ravens, "Gaussian process regression for Arctic coastal erosion forecasting," *IEEE Trans. Geosci. Remote Sens.*, vol. 57, no. 3, pp. 1256–1264, Mar. 2019.

[13] S. Vitousek, P. L. Barnard, P. Limber, L. Erikson and B. Cole, "A model integrating longshore and cross-shore processes for predicting long-term shoreline response to climate change," *J. Geophys. Res., Earth Surf.*, vol. 122, no. 4, pp. 782–806, 2017.

[14] J. W. Long and N. G. Plant, "Extended Kalman filter framework for forecasting shoreline evolution," *Geophys. Res. Lett.*, vol. 39, pp. 1–6, Jul. 2012.

[15] M. L. Yates, R. T. Guza, and W. C. O'Reilly, "Equilibrium shoreline response: Observations and modeling," *J. Geophys. Res., Oceans*, vol. 114, no. C9, 2009.
[16] C. Porter *et al.*, "ArcticDEM," Harvard Dataverse, V1, 2018.
[17] P. Athanasiou, A. Van Dongeren, A. Giardino, M. Vousdoukas, S. Gaytan-Aguilar, and R. Ranasinghe, "Global distribution of nearshore slopes with implications for coastal retreat," *Earth Syst. Sci. Data*, vol. 11, no. 4, pp. 1515–1529, 2019.
[18] P. Bruun, "The Bruun rule of erosion by sea-level rise: A discussion on large-scale two-and three-dimensional usages," *J. Coastal Res.*, vol. 4, pp. 627–648, 1988.
[19] F. M. White, M. L. Spaulding, and L. Gominho, "Theoretical estimates of the various mechanisms involved in iceberg deterioration in the open ocean environment," Rhode Island Univ., Kingston, RI, USA, Tech. Rep. CG-D-62-80, 1980.
[20] D. S. Russell-Head, "The melting of free-drifting icebergs," *Ann. Glaciol.*, vol. 1, pp. 119–122, 1980.
[21] N. Kobayashi, "Formation of thermoerosional niches into frozen bluffs due to storm surges on the Beaufort Sea coast," *J. Geophys. Res., Oceans*, vol. 90, no. C6, pp. 11983–11988, 1985.
[22] P. R. Gent *et al.*, "The community climate system model version 4," *J. Climate*, vol. 24, no. 19, pp. 4973–4991, 2011.
[23] S. M. Griffies *et al.*, "The GFDL CM3 coupled climate model: Characteristics of the ocean and sea ice simulations," *J. Climate*, vol. 24, no. 13, pp. 3520–3544, 2011.
[24] G. A. Schmidt *et al.*, "Present-day atmospheric simulations using GISS ModelE: Comparison to in situ, satellite, and reanalysis data," *J. Climate*, vol. 19, no. 2, pp. 153–192, 2006.
[25] J.-L. Dufresne *et al.*, "Climate change projections using the IPSL-CM5 earth system model: From CMIP3 to CMIP5," *Climate Dyn.*, vol. 40, no. 9/10, pp. 2123–2165, 2013.
[26] S. Yukimoto *et al.*, "The new Meteorological Research Institute coupled GCM (MRI-CGCM2)—Model climate and variability," *Papers Meteorol. Geophys.*, vol. 51, no. 2, pp. 47–88, 2001.
[27] W. V. Sweet *et al.*, "Global and regional sea level rise scenarios for the United States," Center Oper. Oceanograph. Products Serv. Nat. Ocean Serv., Nat. Ocean. Atmos. Admin., Washington, DC, USA, Tech. Rep. NOS CO-OPS 083, 2017.
[28] E. A. Wan and R. Van Der Merwe, "The unscented Kalman filter for nonlinear estimation," in *Proc. IEEE Adapt. Syst. Signal Process., Commun. Control Symp.*, 2000, pp. 153–158.
[29] A. E. Gibbs and B. M. Richmond, "National assessment of shoreline change—Summary statistics for updated vector shorelines and associated shoreline change data for the north coast of Alaska, U.S.–Canadian border to Icy Cape," U.S. Geological Survey, Reston, VA, USA, Open-File Rep. 2017-1107, 2017.
[30] "Planet application program interface: In space for life on earth," Planet, San Francisco, CA, USA, 2017.
[31] Z. Chen, K. Jiang, and J. C. Hung, "Local observability matrix and its application to observability analyses," in *Proc. 16th Annu. Conf. IEEE Ind. Electron. Soc.*, 1990, vol. 1, pp. 100–103.